



The University of
Nottingham

UNITED KINGDOM • CHINA • MALAYSIA

Franza, Andrea and Marshall, Alec M. (2018) Centrifuge modeling study of the response of piled structures to tunneling. *Journal of Geotechnical and Geoenvironmental Engineering*, 144 (2). 04017109/1-04017109/15. ISSN 1943-5606

Access from the University of Nottingham repository:

http://eprints.nottingham.ac.uk/48439/1/Franza%20Marshall_2017_Centrifuge%20modelling%20study%20of%20the%20response%20of%20piled%20structures%20to%20tunnelling%28%29.pdf

Copyright and reuse:

The Nottingham ePrints service makes this work by researchers of the University of Nottingham available open access under the following conditions.

This article is made available under the Creative Commons Attribution licence and may be reused according to the conditions of the licence. For more details see: <http://creativecommons.org/licenses/by/2.5/>

A note on versions:

The version presented here may differ from the published version or from the version of record. If you wish to cite this item you are advised to consult the publisher's version. Please see the repository url above for details on accessing the published version and note that access may require a subscription.

For more information, please contact eprints@nottingham.ac.uk

Centrifuge Modeling Study of the Response of Piled Structures to Tunneling

Andrea Franza¹ and Alec M. Marshall²

Abstract: Tunneling beneath piled structures may compromise the stability and serviceability of the structure. The assessment of potential structure damage is a problem being faced by engineers across the globe. This paper presents the outcomes of a series of geotechnical centrifuge experiments designed to simulate the effect of excavating a tunnel beneath piled structures. The stiffness and weight effects of piled structures are examined independently using aluminum plates of varying stiffness (equivalent beam approach) and the addition of weights supported by aluminum piles. Greenfield displacement patterns and results from pile loading tests are also provided. The variation of structure displacement profiles with plate stiffness, weight, and tunnel volume loss are used to illustrate the main effects of tunnel-pile interaction and the contribution of the superstructure to the global tunnel-pile-structure interaction. Results indicate that piles have a detrimental role in tunnel-structure interaction problems, whereas the superstructure stiffness and weight can, respectively, reduce and increase structure distortions and settlements. Finally, the potential for structural damage is evaluated by comparing structure and greenfield deflection ratios as well as resulting modification factors. The paper presents a unique set of results and insights that provide valuable guidance to engineers working across the ground and structural engineering disciplines. DOI: 10.1061/(ASCE)GT.1943-5606.0001751. This work is made available under the terms of the Creative Commons Attribution 4.0 International license, <http://creativecommons.org/licenses/by/4.0/>.

Author keywords: Tunnel; Pile; Centrifuge modeling; Building response; Settlements; Soil–structure interaction.

Introduction

The development of urban areas has resulted in an increased demand for underground construction that often requires the excavation of tunnels. If protective measures are not adopted, tunneling can pose a threat to the serviceability and ultimate limit state requirements of nearby structures. The use of costly protective measures is often prescribed due to a lack of detailed understanding of the effect of tunneling on structures. In general, engineers need to minimize project costs while preserving structural serviceability and safety.

Most studies related to tunnel-structure interaction (TSI) have considered the case of tunnel construction beneath structures with shallow foundations. Research has shown that structure stiffness tends to decrease tunneling-induced structural distortions with respect to the greenfield case (Mair et al. 1996; Dimmock and Mair 2008; Burland et al. 2004; Amorosi et al. 2014; Fargnoli et al. 2015; Farrell et al. 2014; Son 2015; Camós and Molins 2015; Finno et al. 2005; Losacco et al. 2014; Namazi and Mohamad 2013), and that an increase in the structure weight results in an increase of the potential for damage (Giardina et al. 2015). It has also been shown that deflections are mostly dependent on structural bending stiffness, whereas axial strains depend on

structural axial stiffness (Potts and Addenbrooke 1997; Franzius et al. 2006).

For structures on shallow foundations, preliminary methods to assess tunneling-induced damage have been proposed, including the limiting tensile strain method (Burland et al. 1977; Boscardin and Cording 1989; Mair et al. 1996) and the modification factor approach (Potts and Addenbrooke 1997; Franzius et al. 2006; Giardina et al. 2015).

In the limiting tensile strain method, the structure deflection ratio, DR (Fig. 1), and the horizontal strains, ε_h , are used to calculate the maximum tensile strain in the structure that is compared with limiting strain values associated with a category of damage. Therefore, DR and ε_h may be considered as indicators of deformations. The greater the value of these parameters, the higher the potential for damage. The work presented in this paper focuses on DRs because horizontal strains are negligible for continuous buildings, which is the structural configuration considered in this paper.

In the modification factor approach, to approximately estimate tunneling-induced structural deformations at a preliminary design stage, maximum DR and maximum horizontal strain, ε_h , caused by tunneling are related to surface greenfield movements through the modification factor, M . The modification factor is the ratio between the structure sagging and hogging deformation parameter and the value calculated with respect to the greenfield ground movement profile, as shown in Fig. 1 for M^{DR} . Therefore, M greater and lower than unity is associated with deformations higher and lower than the distortions obtained by forcing the superstructure to settle according to a greenfield settlement trough, respectively. If a given scenario is associated with $M = 0$ (a very stiff superstructure), the superstructure responds to tunneling as a rigid body by settling and/or rotating, with no greenfield deformations transmitted to the superstructure. For the sake of simplicity, a structure that spans hogging and sagging zones is commonly considered as two independent structures. The location of the inflection points, i and i_{bldg} , may vary with tunnel volume loss, $V_{L,t}$.

¹Research Associate, Dept. of Engineering, Univ. of Cambridge, Trumpington St., Cambridge CB2 1PZ, U.K.; formerly, Dept. of Civil Engineering, Faculty of Engineering, Univ. of Nottingham, University Park, Nottingham NG7 2RD, U.K. ORCID: <https://orcid.org/0000-0002-8510-0355>. E-mail: andreafranza@gmail.com

²Associate Professor, Dept. of Civil Engineering, Faculty of Engineering, Univ. of Nottingham, University Park, Nottingham NG7 2RD, U.K. (corresponding author). E-mail: alec.marshall@nottingham.ac.uk

Note. This manuscript was submitted on November 16, 2016; approved on March 21, 2017; published online on November 28, 2017. Discussion period open until April 28, 2018; separate discussions must be submitted for individual papers. This paper is part of the *Journal of Geotechnical and Geoenvironmental Engineering*, © ASCE, ISSN 1090-0241.

required for equilibrium. An increased rate of pile settlement with tunnel volume loss will be observed at this point, which can be used to define pile failure from a tunneling and geotechnical viewpoint. This is in contrast to the conventional definition of pile failure based on a threshold displacement of 10% d_p (Fleming et al. 2009), which arises from structural serviceability requirements.

When assessing the potential for deformations of piled structures affected by tunneling, there is a lack of guidance to support risk assessments. One approach is to adopt methods developed for shallow foundations because the overall deformation mechanism of a superstructure with a piled foundation would be qualitatively similar to one founded on shallow footings (both surface and subsurface tunneling-induced movements follow approximately Gaussian-shaped settlement troughs). However, the superstructure interaction with the soil is based on different mechanisms in these two scenarios (contact pressures on extended surfaces for shallow foundations versus discrete contact and friction interface zones at a subsurface level in the case of piles); therefore, specific research is still needed to improve tunnel-pile-structure interaction analyses.

Practicing engineers often evaluate tunneling-induced deformations of piled structures with empirical TPI analyses (i.e., assuming a fully flexible structure) relating pile head settlements to subsurface greenfield movements. In particular, based on a linear elastic analysis, Devriendt and Williamson (2011) showed that reasonable results are obtained by assuming pile heads settle according to greenfield values at a depth, z , equal to 2/3 the pile length, L_p . However, estimating the deformations of piled structures with TPI analyses that neglect the contribution of relatively stiff superstructures to the global response may be overly conservative, as illustrated by the case study reported by Goh and Mair (2014). This was also confirmed by Franza et al. (2017) using elastic Winkler-based two-stage analyses, which illustrated the respective roles of tunnel-pile interaction and superstructure characteristics (stiffness, configuration) in the global TPSI problem. In particular, Franza et al. (2017) confirmed that structural stiffness can reduce structure deformations and that flexural superstructure deformations are the main concern when continuous horizontal foundation elements are present at the structure base (because these effectively eliminate the transfer of horizontal strains to the structure).

To extend the modification factor approach to structures with piled foundations, Franza et al. (2017) used the spacing, in the direction of the tunnel, between transverse pile rows to represent the contribution of the superstructure to each pile row and proposed the following relative bending stiffness parameters:

$$\rho_{\text{sag}}^p = \frac{EI}{E_s B_{\text{sag}}^3} \frac{S_{\text{lg}}}{L} \quad \rho_{\text{hog}}^p = \frac{EI}{E_s B_{\text{hog}}^3} \frac{S_{\text{lg}}}{L} \quad [\text{m}] \quad (2)$$

where S_{lg} = longitudinal spacing of transverse pile rows; and $EI(S_{\text{lg}}/L)$ = bending stiffness of the portion of the superstructure corresponding to the considered transverse pile row (in kNm^2). Design charts were suggested to estimate M^{DR} from ρ^p . These design charts account for the greenfield subsurface ground movement distribution described by Loganathan and Poulos (1998) for clays in an undrained condition. Furthermore, these envelopes were obtained with an elastic Winkler-based analysis that does not account for the structure weight, soil nonlinearity, or stiffness degradation.

This paper presents results from a program of geotechnical centrifuge tests that aim to investigate the tunnel-pile-structure interaction problem, in particular the key aspects of the superstructure contribution (stiffness and weight) to the global interaction, and how the modification factor design approach, developed for shallow foundations, can be used for the case of piled foundations. To achieve these aims, piled structures were modeled in the centrifuge

as an equivalent aluminum plate supported by aluminum piles and tests were performed to isolate the respective effects of structure stiffness and weight. The paper provides a description of the experimental equipment and program of tests conducted. Results are then presented that focus on soil and structural deformations. Finally, the bending relative stiffness parameter, ρ^p , is used to compare centrifuge test outcomes with the elastic analysis envelopes proposed in Franza et al. (2017), with limitations of the approach and required improvements highlighted.

Experiment Setup, Preparation, and Procedure

Experiments were performed at 80 times normal gravity (80g) using the University of Nottingham geotechnical centrifuge, thereby replicating a prototype 80 times larger than the model [readers may refer to Taylor (1995) for a background on centrifuge testing]. A greenfield test, pile loading tests, and tests modeling the construction of tunnels beneath piled plates were conducted. The centrifuge package and the model layouts are shown in Figs. 2 and 3, respectively. Results are presented in model scale unless otherwise stated.

Centrifuge Package

The experimental package developed by Zhou et al. (2014) to model the tunneling process under greenfield and plane-strain conditions was used. This centrifuge package includes the centrifuge strong box, soil, model tunnel, and tunnel volume control system. The strong box consists of a stainless steel U-channel, a Perspex front wall, and a back aluminum wall. The inside plan dimensions of the strong box are 640×260 mm and the maximum height of soil within the box is 500 mm. The front wall was made of Perspex to allow the measurement of displacements using digital image analysis. A uniform dry fine silica sand known as Leighton Buzzard Fraction E was used for testing ($d_{50} = 0.122$ mm), therefore results directly relate to tunnels in uniform sandy ground. A 90-mm-diameter model tunnel buried at a depth to axis of 225 mm was used to replicate a prototype 7.2-m-diameter tunnel with 14.4 m of cover ($C/D = 2$). The tunnel comprised a rigid inner core with enlarged ends that was sealed within a flexible rubber membrane [similar to that used by Marshall and Mair (2011)]. A tunnel volume control system comprising an actuator connected to a hydraulic cylinder was used to control the volume of fluid

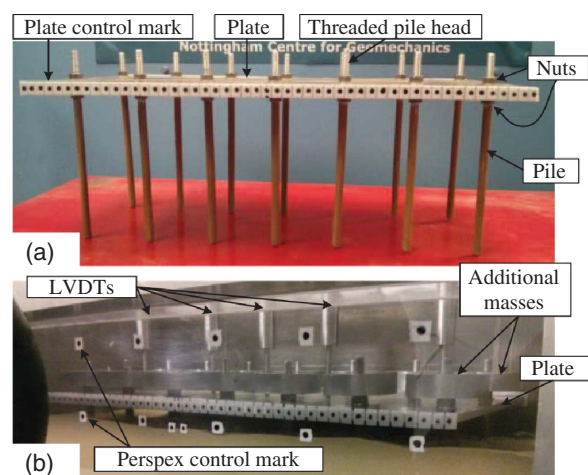


Fig. 2. (a) Model of the piled structure; (b) plate with additional weights

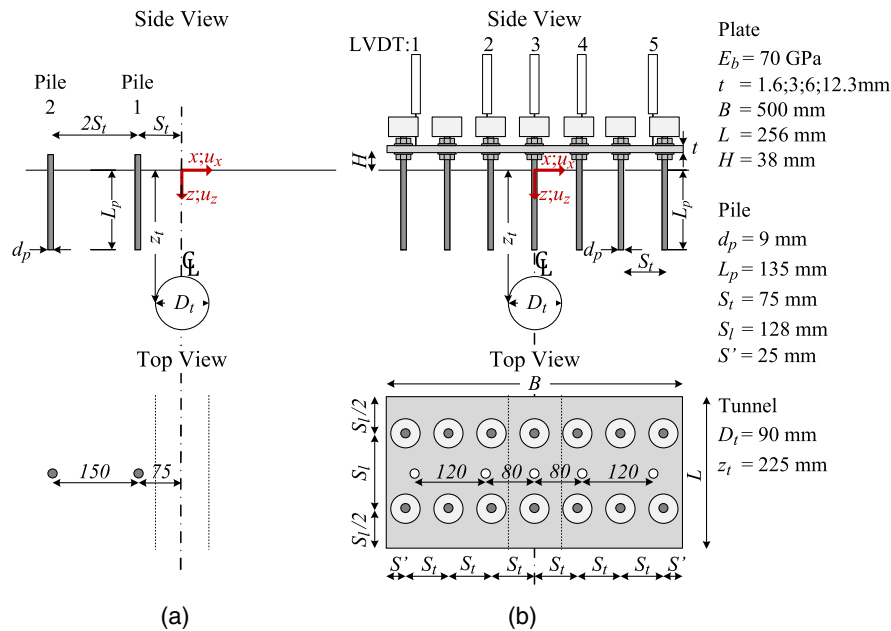


Fig. 3. Test layout (in model scale): (a) loading tests; (b) tunneling beneath piled plate

within the tunnel (a given movement of the cylinder piston correlated to a specific change in tunnel volume). The tunnel volume loss process was conducted in 0.25% increments up to 5% and subsequently in 0.5% increments up to 10%.

Piled structures were modeled using the equivalent beam approach in which aluminum plates with varying stiffness were supported by aluminum piles ($E = 70$ GPa). The plates had a transverse width $B = 500$ mm and a length $L = 256$ mm. Four different plate thicknesses, t , were used: 1.6, 3, 6, and 12.3 mm. The prototype-scale axial and flexural stiffness of these plates (Table 1) encompass most real scenarios, such as the structures monitored during the Jubilee Line Extension (Farrell et al. 2014; Giardina et al. 2015).

The pile foundations, illustrated in Fig. 3(b), consist of transverse rows of seven 8-mm-diameter, flat-bottomed, aluminum alloy rods spaced at a distance of $S_l = 128$ mm along the structure length ($L = 256$ mm). Piles were given a fully rough interface by bonding fraction E sand to the outer surface, resulting in a final diameter of 9 mm over the embedment depth of 135 mm. A gap of $H = 38$ mm existed between the plate and the soil; therefore, the model replicates a piled foundation rather than a piled-raft foundation. The piles were rigidly connected to the plate by bolting the upper (threaded) portion of the piles to the plate. Additional masses could be attached to the threaded upper portions of the piles. Pile loading tests [Fig. 3(a)] were conducted by continuously jacking equivalently prepared piles into the soil.

Table 1. Stiffness of the Aluminum Plates

Test	Model scale		Prototype			
	t (mm)	S_l (mm)	t (m)	S_l (m)	EI^* (kN m ² /m)	EA^* (kN/m)
t1	1.6	128	0.13	10.24	1.2×10^4	9.0×10^6
t3	3	128	0.24	10.24	8.1×10^4	1.7×10^7
t6	6	128	0.48	10.24	6.5×10^5	3.4×10^7
t12	12.3	128	0.98	10.24	5.6×10^6	6.9×10^7

Note: EI^* = parameters evaluated per running meter of structure.

Two Canon PowerShot G10 14.7 MP digital cameras were used to take pictures of the soil (during the greenfield test) and the front face of the plate at each increment of $V_{l,t}$. Displacements were measured from the digital images using *GeoPIV* (White et al. 2003). Plate settlements were also monitored with a row of five LVDTs located along the middle of the strong box, as shown in Fig. 3.

Test Plan and Tested Configurations

The tests conducted for pile loading and tunneling beneath piled plates are illustrated in Figs. 3(a and b), respectively, and summarized in Table 2. Group A consists of a greenfield test; Group B are the loading tests used to characterize the pile load-settlement curve and ultimate pile capacity; Groups C and D investigated the response of piled structures to tunneling. In Group C [presented in Franza and Marshall (2016)], as a result of the varying plate thickness, the weight of the structure also varied between tests, which has been shown to have an effect on the tunnel-structure interactions (Giardina et al. 2015). Therefore, Group D tests were performed with additional masses attached to the tops of the piles (which do not affect the bending stiffness of the model structure). The additional masses were chosen to achieve a specific total weight of the superstructure, enabling a comparison of structures with the same weight but varying stiffness. The value of this specific total weight was selected to obtain a pretunneling safety factor of the foundation (i.e., 2.3) that is within the range of typical design values. Comparison of Groups C and D tests performed with the same plate thickness illustrates the effects of structure weight. Groups C and D tests are labeled according to the plate thickness and structure weight (e.g., t3.w12 refers to a 3-mm-thick plate with masses added to match the weight of the 12-mm-thick plate). Several tests were repeated three times in order to confirm repeatability of results (i.e., tests LP and tests t3 and t6 of Group C); these are indicated with a, b, or c after the test name. Finally, note that the spatial reference system and sign conventions for tunneling-induced displacements are bolded arrows in Fig. 3.

Table 2. Summary of Centrifuge Tests Performed at 80g with Model-Scale Dimensions

Test group	Name (number of tests)	Plate t (mm)	Plate mass (kg)	Pile extra mass (kg)	Total weight ^a (N)	Note
A	GF (1)	—	—	—	—	Greenfield
B	SP (3)	—	—	—	—	Pile loading
C	t1 (1)	1.6	0.55	0	398	Plate
C	t3 (3)	3	1.03	0	745	Plate
C	t6 (3)	6	2.05	0	1,491	Plate
C	t12 (1)	12.3	4.21	0	3,056	Plate
D	t1.w12 (1)	1.6	0.55	0.26	3,056	Plate + weights
D	t3.w12 (1)	3	1.03	0.23	3,056	Plate + weights
D	t6.w12 (1)	6	2.05	0.15	3,056	Plate + weights

^aWeight computed considering the variation of g -level within the centrifuge model.

Model Preparation and Testing

The preparation and testing of the tests considering tunnels beneath piled structures (Groups C and D) were as follows:

1. With the experimental package mounted on the centrifuge, the sand was manually poured to a relative density, I_d , of $30 \pm 5\%$, starting from the tunnel springline level. The effect of sand pouring only above the tunnel springline was considered negligible because previous greenfield centrifuge tests displayed that tunnel deformations were localized above the top half of the model tunnel.
2. The plate (including piles) was pushed into the ground at 1g (therefore representing nondisplacement piles because they were not installed under prototype stress conditions). The pile connections to the stiff plates ensured pile verticality during installation (except for the 1-mm-thick plate in Test t1 in which another stiffer plate was placed against the tops of the piles during installation).
3. The model was spun to 80g.
4. The tunneling simulation process was initiated and measurements made.
5. Upon test completion, the centrifuge was spun down, the piled plate and sand (to a depth of z_t) were removed, and the model tunnel was refilled with the water extracted during Stage 4. The procedure for greenfield tests (Group A) was similar except that Stage 2 was omitted.

For the pile loading tests (Group B)

1. The sand was prepared as previously described.
2. Two piles were pushed at 1g to a depth L_p (again, representing nondisplacement piles). Piles were first manually pushed approximately 40 mm into the soil while checking for verticality, then driven to the design depth using a vertically guided bar, which was also used in flight to apply vertical loads by means

of a load actuator. The two piles were located at the middle of the box width and at an offset from the tunnel of 75 and 225 mm. The spacing between piles ($\approx 17d_p$) is greater than $10d_p$; therefore it should be sufficient to avoid interaction effects (Bolton et al. 1999).

3. The model was spun to 80g, at which point the model tunnel was isolated from the tunnel volume control system.
4. The piles were jacked in flight to get the load-displacement response of the nondisplacement piles.

Centrifuge Modeling Results

Greenfield Test

Greenfield ground movements are often used as an input or reference for soil-structure interaction analyses. This section presents data and a brief discussion of the data obtained from the greenfield test (GF, Group A). These data are incorporated into the modification factor analysis approach presented subsequently.

Contour plots of the greenfield displacements are displayed in Fig. 4 for a $V_{l,t}$ of 1 and 5%, which represents the investigated range of volume losses and corresponds to a typical and a very high value of volume loss encountered in practice. Displacements are normalized by $R \times V_{l,t}$; this normalization enables the identification of changes in displacement mechanisms as volume loss increases. Fig. 4 shows (1) the concentration of ground settlements at the tunnel crown, which implies a narrowing of the settlement trough shape with depth, (2) the settlement trough shape becomes narrower with tunnel volume loss, (3) the magnitude of vertical movements is greater than horizontal displacements (a different scale is adopted in the plots), and (4) horizontal displacements

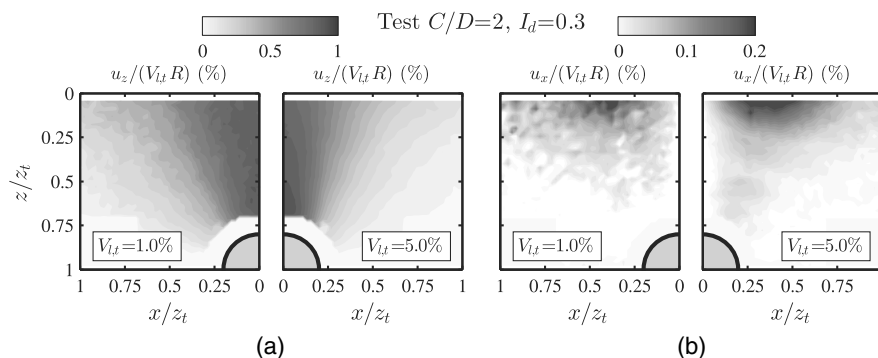


Fig. 4. Greenfield distributions of tunneling-induced (a) vertical; (b) horizontal soil movements at $V_{l,t} = 1$ and 5%

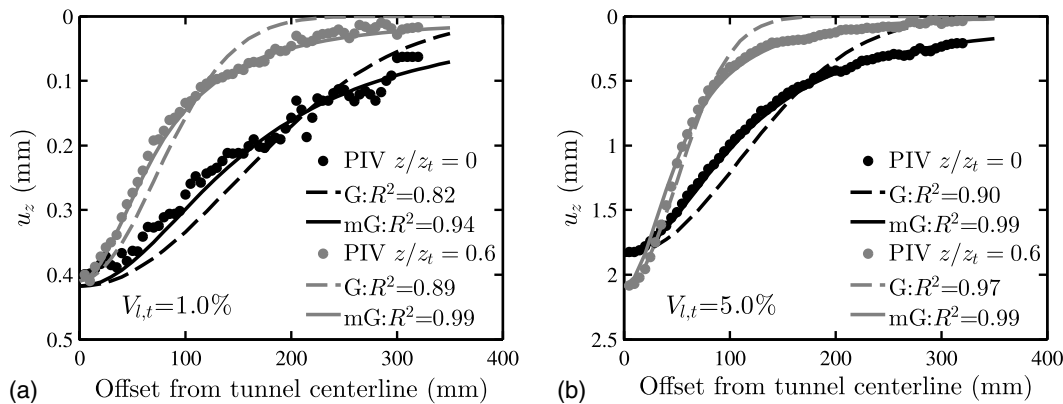


Fig. 5. Curves fitted to settlement data from greenfield test at $z/z_t = 0$ and 0.6 for $V_{l,t} =$ (a) 1%; (b) 5% (G = Gaussian; mG = modified Gaussian)

are mostly noticeable near the surface and negligible at greater depths.

Settlement data are commonly interpolated with empirical curves in order to quantify the effect of tunneling-related parameters on settlement trough shape. In Fig. 5, centrifuge data [particle image velocimetry (PIV)] of settlements at the surface $z/z_t = 0$ and a depth $z/z_t = 0.6$ (corresponding to the pile tip level in test groups C and D) were curve-fitted with Gaussian (G, dashed lines) and modified Gaussian (Vorster et al. 2005) curves (mG, solid lines) for $V_{l,t} = 1$ and 5%. The figure shows that the greenfield settlements were best fitted using modified Gaussian curves (higher coefficients of determination, R^2), which is in agreement with Vorster et al. (2005) and Marshall et al. (2012). Analysis of the fitted curve parameters over the full range of volume loss data illustrated a narrowing of settlement trough shape with $V_{l,t}$; this result, for loose sands, agrees with that of Marshall et al. (2012) for dense sands (settlement shape does not vary considerably with $V_{l,t}$ in clays). Furthermore, the variation of settlement trough shape with relative depth z/z_t is also affected by relative density due to the complex contractive and dilative behavior of the soils [this is elaborated on in Franza (2016) and Zhou et al. (2014)].

Load-Settlement Curve of Single Piles

Pile load tests (Group B) were performed to determine the ultimate pile capacity of the model piles prior to tunneling in order to assess the initial safety factor of the pile foundation. The load-displacement response of nondisplacement piles was assessed from three tests with the same configuration (to check repeatability), as shown in Fig. 6. The existence of the tunnel appears to have some effect (P1, which is close to the tunnel, shows slightly lower forces than P2), however results from the two pile locations are generally consistent. The ultimate capacity of an isolated pile was assumed to be 495 N, the average load obtained at a pile head settlement of $10\%d_p$ (Fleming et al. 2009).

Evaluation of Foundation Initial Safety Factor

It is useful to describe a pile's working load using the initial (i.e., pretunneling) safety factor. This is an important parameter that assesses the initial capacity of the system relative to a state of pile failure. For each test, the initial safety factor of the foundation, SF_0 , was computed as the ratio between the ultimate load capacity of the pile group and the total weight of the superstructure (accounting for the reduced g -level of $74g$ at the level of the plate). The ultimate load capacity of the pile group foundations in test Groups C and D was evaluated as the sum of the ultimate load capacity of each pile

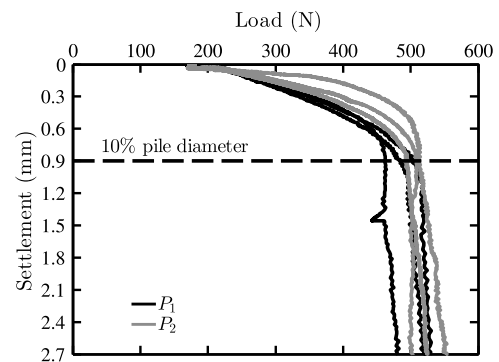


Fig. 6. Measured load-settlement curves of single piles during test group B; the locations of Piles P1 and P2 are illustrated in Fig. 3(a)

(495 N, based on Group B tests). This approach is valid because the pile spacing is more than $8d_p$ and the pile length to diameter ratio, L_p/d_p , is 15, hence block failure (likely for closely spaced slender piles) is not expected (Fleming et al. 2009).

Table 3 shows that the initial safety factor SF_0 ranged between 17.4 and 2.3. In particular, the configurations that tested plates of varying stiffness and constant weight (t12 and Group D) have a $SF_0 = 2.3$, indicative of a common foundation design. The tests with $SF_0 > 2.3$ represent more oversized foundations, hence pile failure is unlikely to be induced by the stress relief caused by tunneling.

Effect of Superstructure Stiffness

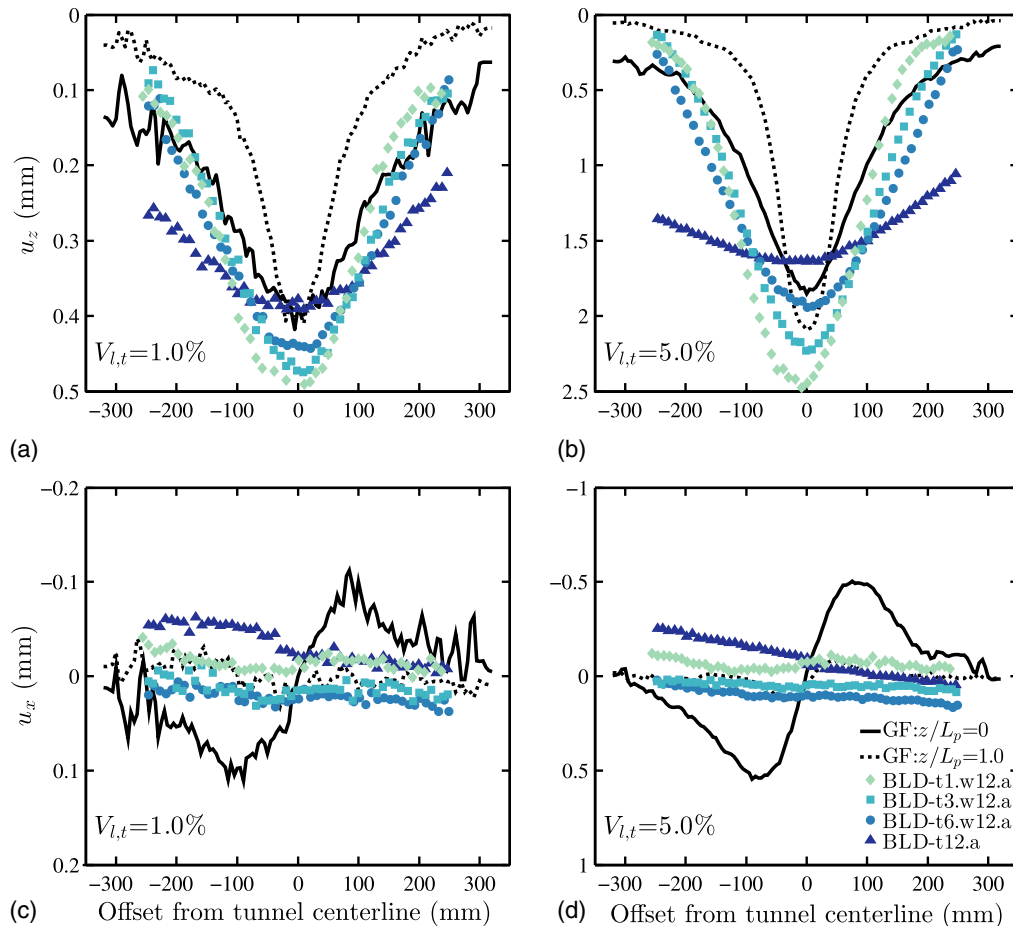
In this paper, a color scheme was adopted in figures that plot results for varying plate thickness: the darker the color, the thicker or stiffer the plate or structure. A comparison of the vertical (u_z) and horizontal (u_x) displacements of the plates with varying stiffness and constant weight ($SF_0 = 2.3$) is presented in Fig. 7. These displacements were measured at $V_{l,t} = 1$ and 5%. For comparison, greenfield (GF) displacements at $z = 0$ and $z/L_p = 1$ are also shown with black lines (the variation of greenfield displacements from the depth of the pile tip to the surface was approximately linear). Structure displacements were approximately symmetric except for Tests t12 and t1.w12, which showed higher displacements on the left side and a global horizontal translation of the plate toward the right (i.e., linear trend of horizontal movements with x). *GeoPIV* measurements of greenfield settlements of low magnitude (i.e., at low volume loss or near the edges of the settlement trough)

Table 3. Initial Safety Factor, SF_0 , of Pile Foundation in Test Groups C and D

Test group	Name (number of test)	Plate thickness (mm)	Plate mass (kg)	Pile mass (kg)	Total weight ^a (N)	Pile capacity (N)	SF_0^b
C	t1 (1)	1.6	0.55	0	398	495	17.4
C	t3 (3)	3	1.03	0	745	495	9.3
C	t6 (3)	6	2.05	0	1,491	495	4.6
C	t12 (1)	12.3	4.21	0	3,056	495	2.3
D	t1.w12 (1)	1.6	0.55	0.26	3,056	495	2.3
D	t3.w12 (1)	3	1.03	0.23	3,056	495	2.3
D	t6.w12 (1)	6	2.05	0.15	3,056	495	2.3

^aWeight computed considering the variation of g -level within the model.

^bPile group safety factor.

**Fig. 7.** Vertical and horizontal displacements of soil (greenfield test) and piled plates for a given structure weight

show some scatter, which is generally less than 0.05 mm. This scatter does impact some subsequent interpretations; however, its effect is not significant.

To identify the key effect of TPI, it is necessary to analyze the response of flexible superstructures, where the superstructure influence is modest (it is not possible to completely exclude its effects because a pile group with a free-head condition was not tested nor were pile head loads measured). The settlement curves of t1.w12 and t3.w12 are characterized by having both hogging and sagging regions. Furthermore, the settlements of the structure in both cases are equal to or greater than the greenfield movements at the pile tip depth; the structure settlement curves are

not intermediate between the $z = 0$ and $z/L_p = 1$ greenfield settlement troughs. These outcomes show that the TPI mechanism is a combination of the interaction of the piles with subsurface ground movements along their lengths and the additional settlements required to remobilize capacity, causing pile settlements to be greater than greenfield values. Additionally, because piles with their tips above the tunnel settle more than the greenfield surface and piles outside this region settle less than the greenfield surface, there is an increase of the relative deflection of more-flexible piled foundations compared with shallow foundations (which would approximately deform according to surface greenfield settlement troughs).

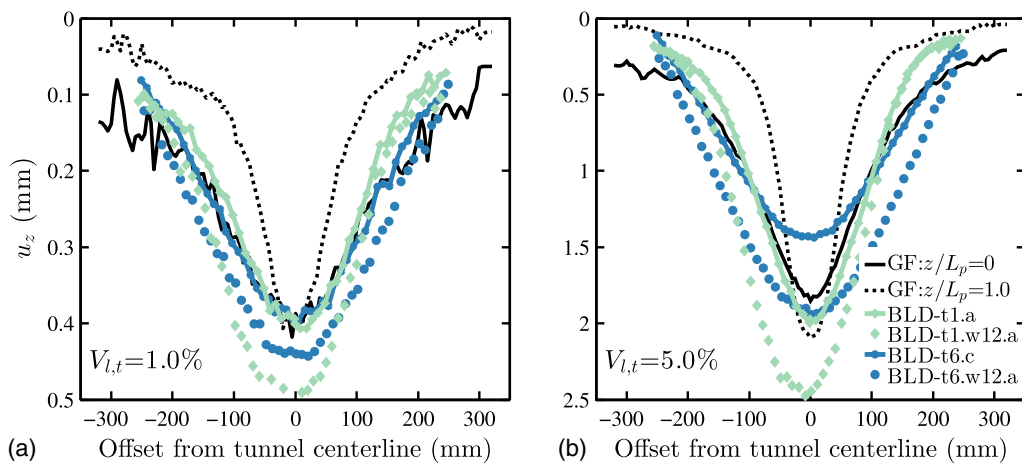


Fig. 8. Vertical displacements of soil (greenfield test) and piled Plates t1 and t6 with varying structure weight

The effects of TPSI can be obtained by examining the stiffer structures, t6.w12 and t12. The data for Test t12 show the following effects: (1) a reduction of the plate relative deflection, Δ , and (2) a decrease of the portion of the plate undergoing hogging deformations due to the increase of i_{blde} (defined in Fig. 1) for structures centered above the tunnel. Effect 1 is due to the plate's ability to resist the central deflection through its own stiffness and the capacity of the outer piles furthest from the tunnel. To restrain tunneling-induced downward movement of the central piles, the plate acts to reduce pile loads (i.e., it applies tensile axial reaction forces), resulting in a reduced pile settlement relative to an isolated pile scenario. This mechanism is similar to the scenario resulting from soil movements inducing negative friction along the shaft of a pile with constrained pile head movements. Due to its stiffness, the plate redistributes loads to the outer piles, which are consequently driven into the soil. If the structure is sufficiently stiff, the load redistribution may result in failure (i.e., $SF = 1$) of the outer piles, resulting in large vertical displacements of the entire foundation, as can be seen for Test t.12. This can be compared against Test t6.12, whose lesser stiffness is not capable of redistributing loads to the outer piles to a degree sufficient to cause pile failure. Effect 2 was also noted by Farrell et al. (2014), who performed centrifuge tests to study the deformations induced by tunneling on an equivalent plate, and Franza et al. (2017) for an equivalent piled beam. Overall, Effects 1 and 2 result in a reduction of structure distortions with plate stiffness, however load redistribution due to a stiff foundation or structure may result in significant overall settlements. Therefore, tunneling may pose a threat to the serviceability state of rigid piled structures in terms of absolute displacements (and tilting in the case of structures not centered above the tunnel).

Figs. 7(c and d) show the horizontal displacements of the plates, which confirm that the axial stiffness of the plate prevents significant horizontal strains of the superstructure (i.e., approximately a linear trend of displacement with offset x) and only marginal horizontal differential displacements arise for the flexible plate t1.w12. In general, the distribution of horizontal strains was negligible across the entire data set (Groups C and D). These outcomes agree with the findings of previous research, which indicate negligible horizontal strains for structures on continuous footings (Burland et al. 2004; Franzus et al. 2006; Farrell et al. 2014). However, these conclusions should not be generalized to structures that do not have horizontal structural elements connecting the pile heads (Goh and Mair 2014; Franza et al. 2017).

Effect of Structure Weight

Fig. 8 shows the effect of structure weight on the settlement of Plates t1 and t6 at medium- and high-volume losses. The effect of structure weight can be evaluated by comparing tests with the same plate thickness but varying weight (e.g., t1 compared with t1.w12) because the additional weight does not contribute to structure stiffness. For Tests t1.w12 and t6.w12, the initial safety factor SF_0 is 2.3, whereas for Tests t1 and t6, $SF_0 = 17.4$ and 4.6, respectively. The effect of structure weight on the TPI can be evaluated for the more flexible t1 tests; the t6 tests indicate the global TPSI. The percentage increase in SF_0 is different for the two plates; therefore, the comparison of the settlement increase between Plates t1 and t6 is only qualitative. In this figure, the greenfield settlement troughs at $z = 0$ and $z/L_p = 1$ are also plotted.

The results illustrate the importance of structure weight in TPSI problems, with greater structure weights producing higher settlements, especially in the sagging zone. Three aspects characterizing the results in Fig. 8 can be noted: (1) The zone of influence tends to be narrower for the flexible structure t1 than for the relatively rigid structure t6; this is due to the difference in bending stiffness between the two plates [Fig. 8(b), Test t1.w12 displays larger settlements than Test t1 between $x = -200$ and $+100$ mm, whereas the entire plate in Test t6.w12 settled more than in test t6]; (2) overall, the shape of the settlement curves is not highly affected by the structure weight; and (3) the increase in vertical displacements due to structure weight is larger at $V_{l,t} = 5\%$ than at $V_{l,t} = 1\%$. This response was also shown for tunnel-single pile interaction in Franza and Marshall (2017b), who showed that the settlement-volume loss curves of single piles under different vertical loads tended to diverge at high tunnel volume loss (i.e., nondisplacement piles with lower SF_0 fully mobilize shaft capacity at lower $V_{l,t}$ than piles with higher SF_0 , whereupon they require larger settlements to mobilize base capacity). The increase in settlements with structure weight is probably associated with two phenomena that have opposing effects: (1) there is an increase in the relative deflection of the plate, Δ (i.e., increase of structure deformations); and (2) there is a higher level of soil stiffness degradation, which results in an increase of the relative stiffness of the superstructure compared with the foundation-soil system. Therefore, to assess the impact of structure weight on deformations and identify the predominant phenomenon, it is necessary to analyze the variation of deformation parameters, DR and M^{DR} , in the sagging and hogging zones (carried out in the following sections). Finally, the results of Test t1 (flexible plate of negligible weight) suggest that the use of

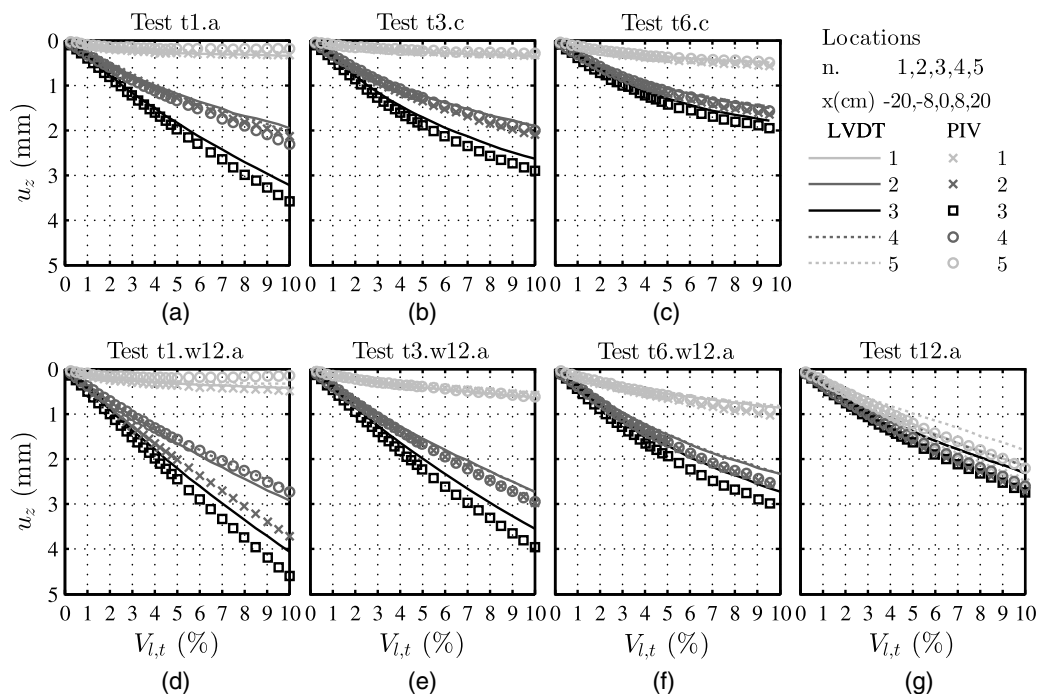


Fig. 9. Plate settlement versus $V_{l,t}$ curves for varying structure weight and stiffness

single-pile settlements within the range of greenfield values between $z/L_p = 0$ and 1, which would be predicted by a linear elastic tunnel-pile interaction analysis (Devriendt and Williamson 2011), is only valid for unloaded piles or foundations with high SF_0 .

Superstructure Deformations and Settlements

Plate Settlement–Volume Loss Curves

Fig. 9 plots vertical displacements against $V_{l,t}$ for the tests in Groups C and D at Locations 1–5 (refer to Fig. 3). Image analysis (PIV) results taken at the Perspex wall and LVDT measurements made within the middle of the centrifuge container are presented. None of the plates experienced a brittle failure (i.e., a sharp increase in the rate of settlement), which was previously shown for the case of tunnel–single pile interaction in sand (Marshall and Mair 2011). This is due to two factors: (1) the use of nondisplacement piles, whose tunneling-induced settlement–volume loss curve for isolated piles with constant loads is not as steep as for displacement piles (Franza and Marshall 2017b), and (2) the load redistribution between piles, which depends on the superstructure (plate) stiffness and the magnitude of differential displacements between adjacent piles (although the thickness of Plate t1 results in a low bending stiffness, EI , the load redistribution may be relevant because of the large differential pile displacements). To understand the latter component, a comparison can be made to a simply supported beam loaded by a unit force at its midpoint. The maximum settlement of the beam is proportional to the cube of the span length and the inverse of EI . Therefore, the narrower the settlement trough (which may result from an initial loss of capacity of the central piles), the greater the load redistribution (which acts to limit the failure or movement of the central piles).

The results in Fig. 9 illustrate the influence of superstructure properties on the change of rate of settlement of the plates with $V_{l,t}$. The results in Figs. 9(d–g) for a consistent structure weight illustrate a small reduction of the rate of settlement with $V_{l,t}$, which

is more marked for Test t6.w12 than for Tests t3.w12 and t1.w12 (which are approximately linear). This reduction of the rate of settlement with $V_{l,t}$ is probably due to slippage between the pile and soil and ground stiffness degradation due to tunneling and TPSI mechanisms (i.e., the structure displaces the piles because of its own stiffness with respect to the soil, inducing slippage between pile and soil and additional shearing strains at the soil-pile interface). The stiffer the structure, the greater the soil degradation and slippage. On the contrary, the rate of settlement in Test t12 is almost constant [Fig. 9(g)]; this is probably due to the combined effects of superstructure stiffness and load redistribution from the central to the outer piles (causing the outer piles to be driven into the soil as their load capacity is exceeded). Once the outer piles reach their ultimate capacity, further increments of $V_{l,t}$ result in a global settlement of the pile and plate system to satisfy the equilibrium condition of the piles. The tests performed with constant plate thickness but different SF_0 are compared in Figs. 9(a and d), (b and e), (c and f); the data show a greater reduction of the rate of settlement (especially at high $V_{l,t}$) for the lower structure weights.

In general, comparison of Figs. 9(a and g) illustrates that the settlement variation of the central piles (solid black lines) induced by structure stiffness and weight is lower than for the outer piles (solid and dashed light gray lines). This has as direct consequence that the structure deformations (as DRs) are highly affected by the superstructure weight and stiffness, whereas the superstructure has a less significant impact on the maximum settlements of the structure.

Relationship between Maximum Plate and Greenfield Settlements

The maximum structure settlement is important for the assessment of damages related to the serviceability limit state. In this and subsequent sections, the greenfield ground movements are analyzed at normalized depths of $z/L_p = 0$ and $2/3$ to compare results of TPSI with terms often used in the case of shallow foundations ($z = 0$)

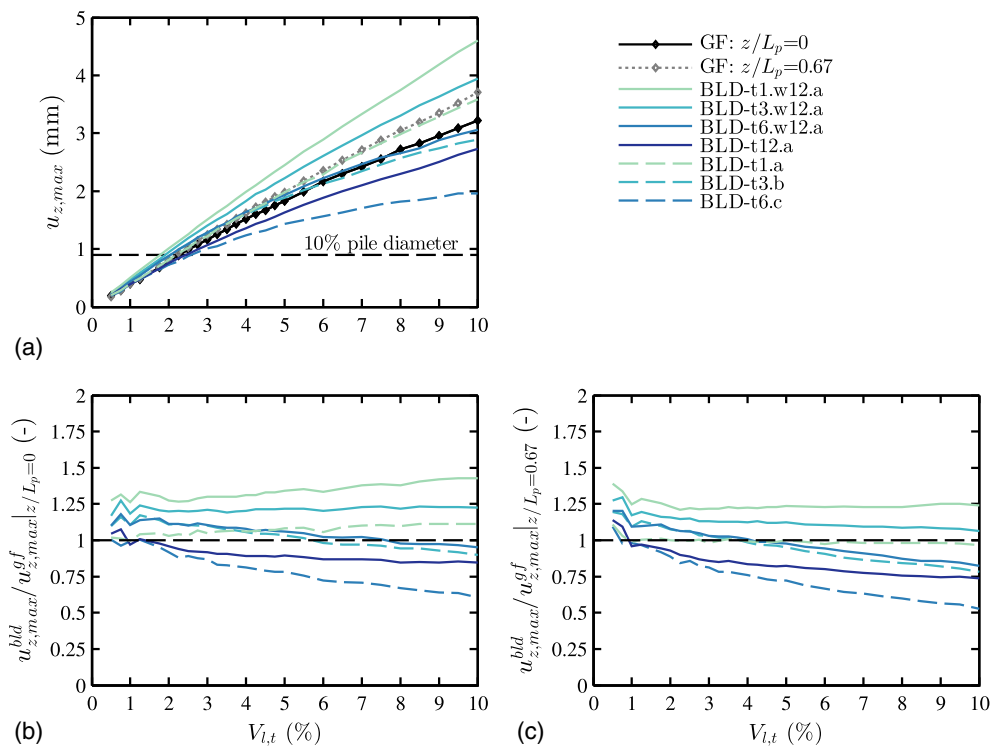


Fig. 10. Influence of the plate self-weight and stiffness on the maximum settlements of the superstructure

and the empirical approach used for piled structures ($z/L_p = 2/3$) (Devriendt and Williamson 2011). To highlight the influence of plate stiffness and structure weight, the maximum settlements measured at each $V_{l,t}$ increment of the plates ($u_{z,max}^{bld}$) and the greenfield settlement troughs ($u_{z,max}^{gf}$) at $z = 0$ and $z/L_p = 2/3$ are displayed in Fig. 10(a), whereas the ratio ($u_{z,max}^{bld} / u_{z,max}^{gf}$) between the plate displacement and the surface and subsurface greenfield settlements is shown in Figs. 10(b and c), respectively. The latter figures are useful to relate the results of the global interaction with greenfield movements, which can be used as a reference term.

Fig. 10(a) confirms that the plate stiffness and weight tend to decrease and increase, respectively, the maximum settlement of the superstructure within the investigated range of $V_{l,t}$. The critical maximum settlement of $10\%d_p = 0.9$ mm is plotted in Fig. 10(a) for guidance. The results also show that the greenfield settlements, $u_{z,max}^{gf}$, vary almost linearly with $V_{l,t}$ and that the critical settlement of 0.9 mm was reached by all the superstructures at $V_{l,t} = 1.5\text{--}2.5\%$, which is a relatively narrow interval. Furthermore, as shown by the solid lines in Figs. 10(b and c), the dimensionless parameter $u_{z,max}^{bld} / u_{z,max}^{gf}$ ranges within the interval 0.75–1.5 (mostly between 0.85 and 1.3) for the constant structure weight cases, confirming a relatively narrow range of variability of the normalized maximum plate settlements. Therefore, if it is unlikely that pile failure will be reached (i.e., $SF > 1$), a preliminary assessment of maximum structure settlement could be carried out using a TPI analysis (i.e., assuming a fully flexible structure) accounting for the superstructure weight; this type of analysis would lead to a conservative but acceptable estimation of structure maximum settlements.

Deflection Ratios

In the modification factor approach, the DR modification factors, M^{DR} (Fig. 1), are used to determine structure DR values from the

greenfield settlement trough. The location of the greenfield and structure inflection points, i and i_{bldg} , may vary with tunnel volume loss, $V_{l,t}$, whereas DR is calculated based on the maximum relative deflection, Δ . In this study, to calculate DR and the location of i and i_{bldg} , the settlement curves of the soil and plates, obtained from test groups A, C, and D, were interpolated using modified Gaussian curves (Farrell et al. 2014; Marshall et al. 2012; Vorster et al. 2005).

The influence of the superstructure and $V_{l,t}$ on DR and M^{DR} is displayed in Figs. 11 and 12, which show, respectively, the effects of the structure stiffness and weight; Figs. 11(a and b) and 12(a and b) show the structure and greenfield DRs in both sagging and hogging, whereas Figs. 11(c and d) show the modification factors, $M^{DR,sag}$ and $M^{DR,hog}$.

The influence of structure stiffness can be seen by examining the structures with a constant SF_0 [triangle-shaped markers in Figs. 11(a and b)]. For the flexible structure test t1.w12, the DR values are intermediate between greenfield surface and subsurface values and distributed approximately along a straight line, which indicates that the piles average the greenfield deformation pattern in terms of deformations. On the other hand, for the centrifuge tests t3.w12, t6.w12, and t12, the data follow nonlinear distributions that are characterized by decreasing values of DR with plate thickness and a gradual decrease of the increment rate with $V_{l,t}$. Although these results are qualitatively similar to the trends of the maximum settlements shown in Fig. 10, the curves in Fig. 11(a) have a marked drop in DR with plate thickness. As discussed previously, the observed nonlinear trend of superstructure deformations with volume loss could be attributed to the progressive degradation of soil stiffness and the relative pile-soil displacements induced by the superstructure.

The effect of structure weight on DR is displayed in Figs. 12(a and b); triangular markers are used for configurations with $SF_0 = 2.3$, whereas square markers are used for structures with higher safety factors (lower weights). For all cases, in the sagging zone, the deflection ratios undergo a notable increase with

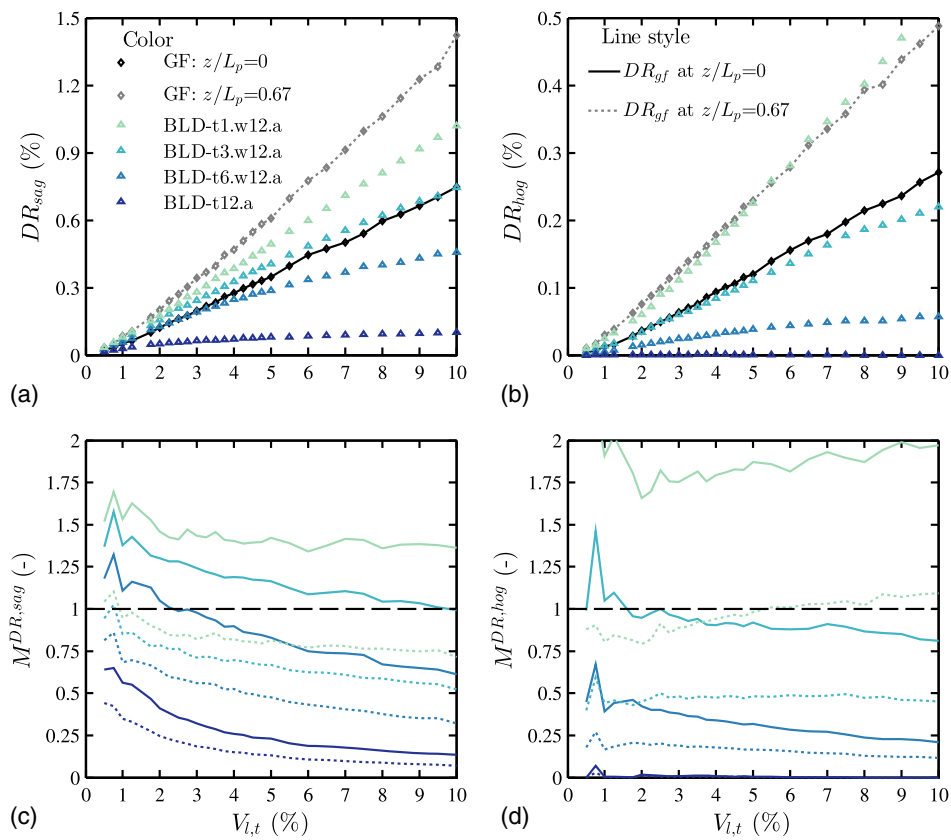


Fig. 11. Effects of structure stiffness: variation of (a and b) DR and (c and d) M^{DR} for Plates t1, t3, t6, and t12 in (a and c) sagging and (b and d) hogging

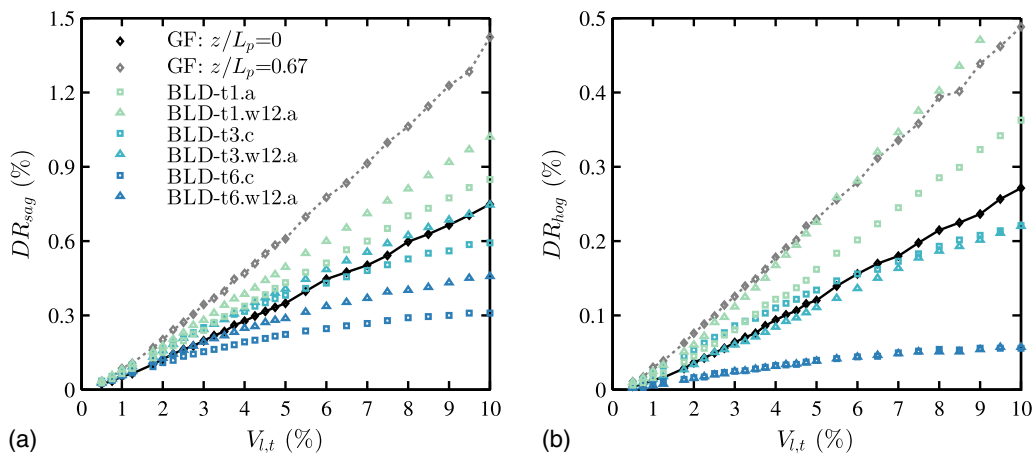


Fig. 12. Effects of structure weight: variation of DR for Plates t1, t3, and t6 in (a) sagging; (b) hogging

structure weight (i.e., reduction of SF_0). In the hogging zone, this increase only occurs for the flexible Plate t1; DR values essentially remain the same for the other cases. In the case of stiff structures, both square and triangular markers (heavy and light structures) follow nonlinear distributions with an asymptotic trend at high volume loss.

Figs. 11(c and d) show the effects of plate stiffness on the reduction factors, $M^{DR,sag}$ and $M^{DR,hog}$, calculated using surface (solid lines) and subsurface (dashed lines) greenfield settlements. The structure weight is constant for the data set in these figures.

The data normalized with greenfield surface DRs (solid lines) show that the TPI mechanism results in M^{DR} values greater than unity for flexible structures, whereas structural stiffness tends to decrease the flexural deformations (as discussed previously). Except for the hogging modification factors, $M^{DR,hog}$, of Test t1 that are approximately constant, Figs. 11(c and d) show that the values of M^{DR} are characterized by a steady decrease throughout the entire range of $V_{l,t}$; the thicker the plate (higher the structural stiffness), the greater the rate of decrease. Furthermore, as displayed by the dashed lines, similar qualitative trends with plate thickness and $V_{l,t}$ were

obtained for the modification factors defined using the subsurface greenfield deformations. However, because greenfield settlement troughs are wider at the surface than at depth, the magnitudes of the dashed lines are considerably lower than the solid lines. The scatter of M^{DR} at low volume loss is caused by the scatter in the greenfield (GF) displacements.

The dashed lines in Figs. 11(c and d) can be used to evaluate the performance of the simplified empirical TPI analyses described by Devriendt and Williamson (2011) based on subsurface greenfield settlement profiles (i.e., DR_{gf} at $z/L_p = 2/3$). The modification factors $M^{DR,sag}$ and $M^{DR,hog}$ related to DR_{gf} at $z/L_p = 2/3$ resulted in values of $M^{DR,sag}$ and $M^{DR,hog} < 1.0$. In particular, during Test t12, $M^{DR,sag} < 0.5$ and $M^{DR,hog} = 0$ for DR_{gf} measured at $z/L_p = 2/3$. Therefore, these data suggest that this damage assessment should be reliable and conservative for $SF_0 > 2.5$ in the case of nondisplacement piles.

Finally, comparison of Figs. 10 and 11 illustrates the different range of variability of the plate normalized maximum settlements and deformations and the need to account for superstructure stiffness in the assessment of piled structure distortions. The following section presents the measured modification factors within the context of previously published design charts relating M^{DR} to relative structure-soil stiffness.

Relative Structure-Soil Stiffness and Modification Factors

In the case of piled foundations, it is not possible to simplify the problem to a plane-strain condition. Therefore, to study the flexural deformations of piled structures using the modification factor framework, the relative structure-soil bending stiffness factor, ρ^p , defined in Eq. (2), was applied. To define ρ^p , it is necessary to assess the bending stiffness, EI , of the portion of structure corresponding to each transverse pile row, the transverse length, B , of the sagging and hogging zones in the greenfield condition, and the soil stiffness E_s . First, the plate was separated into two independent portions in the longitudinal direction to assess EI corresponding to each pile row. The value of B was measured from the surface greenfield settlement curves by identifying the offset of inflection point at each volume loss value, and E_s was estimated from the strains induced by greenfield displacements following the logic of Marshall et al. (2010) and Farrell (2010). The procedure consists of two parts: (1) The stiffness–shear strain relationship for the soil was defined from triaxial test data; and (2) soil shear strains induced by volume loss, γ , were assessed from the displacements measured in the greenfield condition. To account for the spatial variability of E_s , a representative value was assessed at a normalized depth $z/z_t = 0.5$ [as suggested by Franzus et al. (2006) for shallow foundations] to account for the fact that both the soil at the piles and beneath the tip level are involved in the interaction. Additionally, an average shear strain, γ_{avg} , from $\pm 2.5i$ along the settlement trough was used

$$\gamma_{avg}(z, V_{l,t}) = \frac{1}{5i} \int_{-2.5i}^{2.5i} \gamma dx \quad (3)$$

The relationship for $\gamma_{avg} - V_{l,t}$, measured from the greenfield test at a depth $z/z_t = 0.5$, as well as the estimated secant soil stiffness E_{sec} , are shown in Fig. 13; the latter curve displays an exponential reduction of soil stiffness with strain, resulting in an asymptotic trend at high volume losses. Further details on the calculation of shear stiffness are provided in Franzus (2016).

Because of the use of greenfield representative conditions, the structure weight effect on stresses, and thus stiffness, is neglected.

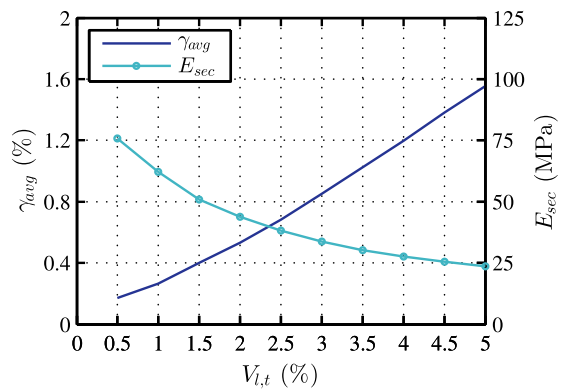


Fig. 13. Average shear strain and soil stiffness with volume loss

The variation of γ due to the presence of piles and the relative pile-soil displacements induced by the structure load redistribution is also neglected. Furthermore, partitioning of the building transverse length into B_{sag} and B_{hog} with respect to the surface (as for shallow foundations) neglects the presence of piles. However, calculation of the relative structure-soil stiffness in this way allows for direct comparison of modification factors, M^{DR} , with those for shallow foundations. Also, the effects of relative stiffness on structure distortions are proportional to a logarithmic scale (Franzus et al. 2006); therefore, the accuracy of its estimation can range within an order of magnitude without introducing significant errors.

Fig. 14 displays the modification factors in sagging and hogging zones, $M^{DR,sag}$ and $M^{DR,hog}$, against the relative bending stiffness ρ^p . The values of $M^{DR,sag}$ and $M^{DR,hog}$ were defined using the measured structure deformations and surface greenfield settlements within the volume loss range of $V_{l,t} = 0.5$ –5%. The envelopes proposed by Franzus et al. (2017) based on the simplifying assumptions of soil linearity and perfect bonding between the pile and soil are also displayed in this figure. The Franzus et al. (2017) design curves were based on soil displacement patterns applicable to undrained clays; therefore, the effects of the different soil deformation patterns obtained for sands in this study on M^{DR} are neglected here. This simplification is to some extent supported by Mair (2013), whose design envelopes for shallow foundations captured data related to both clays and sands.

The results in Fig. 14 show that (1) the increase in relative stiffness decreases the structure deformations (decrease of M^{DR}), (2) the structure weight increases deformations (increases M^{DR}), (3) in the sagging zone, the increase in volume loss results in an increase of ρ_{sag}^p and a decrease of $M^{DR,sag}$, and (4) in the hogging zone, an increase in volume loss causes a decrease in $M^{DR,hog}$ but has little impact on ρ_{hog}^p . The main interaction mechanisms causing these results were described in the previous section, except for the effects of $V_{l,t}$ on ρ^p . Because the structural bending stiffness is constant for a given plate, the changes in ρ^p must be a consequence of changes in $E_s \times B_{sag}^3$ and $E_s \times B_{hog}^3$ with $V_{l,t}$ [Eq. (2)]. The values of E_s , B_{sag} , and B_{hog} were all calculated using greenfield test data; the variation of E_s with $V_{l,t}$ is illustrated in Fig. 13. Values of B_{sag} and B_{hog} depend on the location of the inflection point, i , which decreases with $V_{l,t}$ (i.e., the settlement trough becomes narrower). For instance, ρ_{hog}^p is approximately constant for $V_{l,t} = 0.5$ –5% because the effects of soil stiffness degradation are countered by the increase in B_{hog} . In general, the trends of ρ_{sag}^p and ρ_{hog}^p will be affected by the tunnel-structure eccentricity through the greenfield relationship between i and $V_{l,t}$. Although the Franzus et al. (2017) envelopes are based on the assumption of linear elasticity, perfect soil-pile bonding, and greenfield displacements in undrained clay,

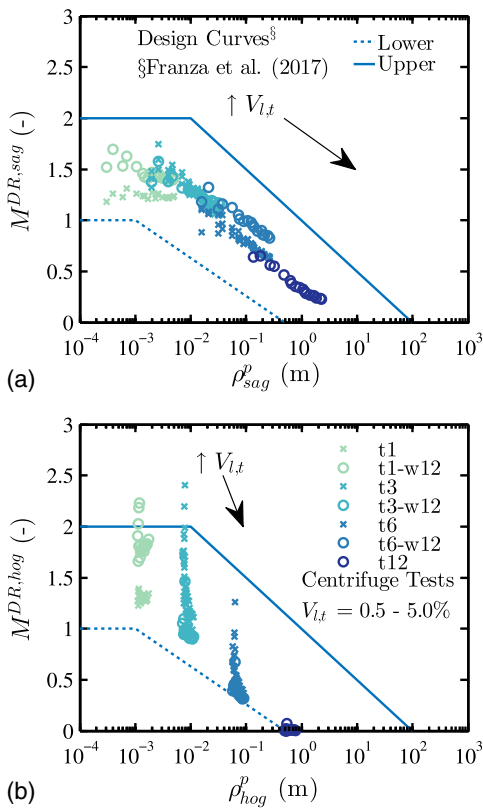


Fig. 14. Comparison between centrifuge results and design lines: M^{DR} computed with respect to surface greenfield settlement troughs versus relative structure stiffness in (a) sagging; (b) hogging

most results fall within the envelopes and, especially for the sagging zone (the primary deformation mode of the structure), the trend of M^{DR} from the centrifuge tests follows that of the upper and lower bounds. Despite the overall agreement, engineers should use appropriate judgment to evaluate the applicability of these design envelopes to real cases of tunnel-building interaction.

Discussion

Several issues related to the adopted centrifuge modeling methodology are noteworthy. First, the load application procedure differs between the pile loading tests (Group B) and the tests that model tunneling beneath a piled plate (Groups C and D). During the loading tests, the pile load was applied after the final g -level was reached; in the latter test groups the foundation load is due to the mass of the superstructure, thus the loads increased throughout the centrifuge spin-up process. Furthermore, the load distribution within the pile group is the result of a soil-structure interaction phenomenon that is influenced by the superstructure stiffness and the pile response during spin-up. Therefore, prior to tunnel volume loss, the superstructure weight may not be uniformly distributed between the piles. Despite these discrepancies, a similar ultimate failure mechanism is expected for the nondisplacement piles in both types of tests.

Second, it is important to stress that the model of tunnel-pile structure interaction does not satisfy the plane-strain condition. The Perspex and back walls approximately represent planes of symmetry; therefore, the centrifuge tests modeled the behavior of an infinitely long structure in the direction of the tunnel (limited

in the model to a portion corresponding to two pile rows) subjected to plane-strain tunnel ground movements.

Finally, the approximations of an equivalent plate approach should be considered. Several studies highlighted the importance of structural configuration and that the use of equivalent plate and beam models for the superstructure may lead to a different structural response, for instance, compared with when they are modeled as framed structures (Goh and Mair 2014; Fargnoli et al. 2015; Franza et al. 2017). On the other hand, it is common practice to simplify the superstructure in this way for centrifuge modeling in order to decrease the experimental complexity. Despite these approximations, this study provided a valuable data set that highlights the main interaction mechanisms involved during tunnel-pile-structure interaction. However, further studies should assess the influence of the structural configuration.

Conclusions

This paper presented results from a series of centrifuge tests performed to study the response of piled structures to tunnel excavation located centrally with respect to the superstructure. The following conclusions can be drawn from the obtained data, which may provide useful guidance to tunnel engineers.

- Centrifuge data confirmed that piled foundations alter the global tunnel-pile-structure interaction with respect to shallow foundations, causing a greater potential for damage of flexible structures. As for shallow foundations, the structure stiffness decreases its distortions (both deflection ratios and horizontal strains); horizontal strains in piled structures that are continuous at the ground level should be negligible.
- Structure settlements are dependent on the relationship between structure stiffness and weight, as well as the safety factor of the piles. The impact of structure weight on settlements is considerable; increased structure weight (for a given stiffness) results in an increase in flexural distortions and, to a lesser extent, maximum settlements above the tunnel. Neglecting the impact of structure weight is not conservative.
- In general, an assessment of the posttunneling pile safety factor should be carried out, considering pile head load redistribution and that pile capacity may be decreased by tunnel volume loss. Attention should be paid to the absolute settlement of rigid structures when loads being redistributed by the superstructure from piles above the tunnel toward external piles exceed their capacity.
- Preliminary damage assessment procedures for piled structures that assume the structure is fully flexible but consider the structure weight (i.e., a tunnel-pile interaction analysis) can lead to an overestimation of structure deflection ratios and horizontal strains, whereas they would result in an acceptable and conservative estimate of maximum settlement if there is no potential for reaching pile failure (i.e., posttunneling $SF = 1$).
- In the tested configurations of nondisplacement piles with pre-tunneling pile safety factor $SF_0 > 2.0$, the assumption that the superstructure deforms as the subsurface greenfield settlement curves at $z/L_p = 2/3$ (which does not account for the structure weight) provided a conservative assessment of the structure DR. However, this conclusion should not be generalized to displacement pile foundations and/or lower SF_0 conditions.
- The distribution of $M^{DR,sag}$ and $M^{DR,hog}$ agreed with previously proposed design envelopes. However, further studies are needed to improve the accuracy and reliability of the assessment method in the case of piled structures, in particular to account for different ground conditions.

Acknowledgments

This work was supported by the Engineering and Physical Sciences Research Council (EPSRC) (EP/K023020/1, 1296878; EP/N509620/1). The research materials supporting this publication can be accessed from Franza and Marshall (2017a).

References

- Amorosi, A., Boldini, D., De Felice, G., Malena, M., and Sebastianelli, M. (2014). "Tunnelling-induced deformation and damage on historical masonry structures." *Géotechnique*, 64(2), 118–130.
- Basile, F. (2014). "Effects of tunnelling on pile foundations." *Soils Found.*, 54(3), 280–295.
- Bolton, M. D., et al. (1999). "Centrifuge cone penetration tests in sand." *Géotechnique*, 49(4), 543–552.
- Boscardin, M. D., and Cording, E. J. (1989). "Building response to excavation-induced settlement." *J. Geotech. Eng.*, 10.1061/(ASCE)0733-9410(1989)115:1(1), 1–21.
- Burland, J. B., Broms, B. B., and De Mello, V. F. B. (1977). "Behaviour of foundations and structures." *Proc., 9th Int. Conf. on Soil Mechanics and Foundations Engineering*, Vol. 2, Japanese Society of Soil Mechanics and Foundation Engineering, Tokyo, 495–546.
- Burland, J. B., Mair, R. J., and Standing, J. R. (2004). "Ground performance and building response due to tunnelling." *Advances in Geotechnical Engineering: The Skempton Conf.*, R. J. Jardine, D. M. Potts, and K. G. Higgins, eds., Vol. 1, Thomas Telford Services, London, 291–344.
- Camós, C., and Molins, C. (2015). "3D analytical prediction of building damage due to ground subsidence produced by tunneling." *Tunnelling Underground Space Technol.*, 50, 424–437.
- Cheng, C. Y., Dasari, G. R., Chow, Y. K., and Leung, C. F. (2007). "Finite element analysis of tunnel-soil-pile interaction using displacement controlled model." *Tunnelling Underground Space Technol.*, 22(4), 450–466.
- Devriendt, M., and Williamson, M. (2011). "Validation of methods for assessing tunnelling-induced settlements on piles." *Ground Eng.*, 2011(Mar), 25–30.
- Dias, T. G. S., and Bezuijen, A. (2015). "Data analysis of pile tunnel interaction." *J. Geotech. Geoenviron. Eng.*, 10.1061/(ASCE)GT.1943-5606.0001350, 04015051.
- Dimmock, P. S., and Mair, R. J. (2008). "Effect of building stiffness on tunnelling-induced ground movement." *Tunnelling Underground Space Technol.*, 23(4), 438–450.
- Fargnoli, V., Gragnano, C. G., Amorosi, A., and Boldini, D. (2015). "3D numerical modelling of soil-structure interaction during EPB tunnelling." *Géotechnique*, 65(1), 23–37.
- Farrell, R. (2010). "Tunnelling in sands and the response of buildings." Ph.D. thesis, Cambridge Univ., Cambridge, U.K.
- Farrell, R., Mair, R., Sciotti, A., and Pigorini, A. (2014). "Building response to tunnelling." *Soils Found.*, 54(3), 269–279.
- Finno, R. J., Voss, F. T., Rossow, E., and Blackburn, J. T. (2005). "Evaluating damage potential in buildings affected by excavations." *J. Geotech. Geoenviron. Eng.*, 10.1061/(ASCE)1090-0241(2005)131:10(1199), 1199–1210.
- Fleming, W. G. K., Weltman, A. J., Randolph, M. F., and Elson, W. K. (2009). *Piling engineering*, 3rd ed., Taylor & Francis, Abingdon, VA.
- Franza, A. (2016). "Tunnelling and its effects on piles and piled structures." Ph.D. thesis, Univ. of Nottingham, Nottingham, U.K.
- Franza, A., and Marshall, A. M. (2016). "Centrifuge modelling of piled structure response to tunnelling." *Proc., 3rd European Conf. on Physical Modelling in Geotechnics (Eurofuge 2016)*, L. Thorel, A. Bretschneider, M. Blanc, and S. Escoffier, eds., IFFSTAR, Nantes, France, 313–318.
- Franza, A., and Marshall, A. M. (2017a). "ASCE_JGGE_A centrifuge modelling study of the response of piled structures to tunneling." (<http://dx.doi.org/10.17639/nott.74>) (May 15, 2017).
- Franza, A., and Marshall, A. M. (2017b). "Centrifuge modelling of tunnelling beneath axially loaded displacement and non-displacement piles in sand." *Proc., Geotechnical Frontiers. GSP 277: Transportation Facilities, Structures, and Site Investigation*, T. L. Branson and R. J. Valentine, eds., ASCE, Reston, VA, 576–586.
- Franza, A., Marshall, A. M., Haji, T., Abdelatif, A. O., Carbonari, S., and Morici, M. (2017). "A simplified elastic analysis of tunnel-piled structure interaction." *Tunnelling Underground Space Technol.*, 61(Jan), 104–121.
- Franzius, J. N., Potts, D. M., and Burland, J. B. (2006). "The response of surface structures to tunnel construction." *Proc. Inst. Civ. Eng. Geotech. Eng.*, 159(1), 3–17.
- GeoPIV [Computer software]. University of Western Australia, Crawley, Australia.
- Giardina, G., DeJong, M. J., and Mair, R. J. (2015). "Interaction between surface structures and tunnelling in sand: Centrifuge and computational modelling." *Tunnelling Underground Space Technol.*, 50(Aug), 465–478.
- Goh, K. H., and Mair, R. J. (2014). "Response of framed buildings to excavation-induced movements." *Soils Found.*, 54(3), 250–268.
- Hong, Y., Soomro, M., and Ng, C. (2015). "Settlement and load transfer mechanism of pile group due to side-by-side twin tunnelling." *Comput. Geotech.*, 64(Mar), 105–119.
- Jacobsz, S. W., Bowers, K. H., Moss, N. A., and Zanardo, G. (2005). "The effects of tunnelling on piled structures on the CTRL." *Proc., 5th Int. Symp. on Geotechnical Aspects of Underground Construction in Soft Ground*, Balkema, Leiden, Netherlands, 115–121.
- Jacobsz, S. W., Standing, J. R., Mair, R. J., Hagiwara, T., and Sugiyama, T. (2004). "Centrifuge modelling of tunnelling near driven piles." *Soils Found.*, 44(1), 49–56.
- Jongpradist, P., et al. (2013). "Development of tunneling influence zones for adjacent pile foundations by numerical analyses." *Tunnelling Underground Space Technol.*, 34(Feb), 96–109.
- Kaalberg, F. J., Teunissen, E. A. H., van Tol, A. F., and Bosch, J. W. (2005). "Dutch research on the impact of shield tunnelling on pile foundations." *Proc., 5th Int. Symp. on Geotechnical Aspects of Underground Construction in Soft Ground*, K. J. Bakker, A. Bezuijen, W. Broere, and E. A. Kwast, eds., Taylor & Francis, Amsterdam, Netherlands, 123–131.
- Kitiyodom, P., Matsumoto, T., and Kawaguchi, K. (2005). "A simplified analysis method for piled raft foundations subjected to ground movements induced by tunnelling." *Int. J. Numer. Anal. Methods Geomech.*, 29(15), 1485–1507.
- Lee, C. J., and Jacobsz, S. W. (2006). "The influence of tunnelling on adjacent piled foundations." *Tunnelling Underground Space Technol.*, 21(3–4), 430.
- Lee, C.-J., and Chiang, K.-H. H. (2007). "Responses of single piles to tunneling-induced soil movements in sandy ground." *Can. Geotech. J.*, 44(10), 1224–1241.
- Loganathan, N., and Poulos, H. G. (1998). "Analytical prediction for tunneling-induced ground movements in clays." *J. Geotech. Geoenviron. Eng.*, 10.1061/(ASCE)1090-0241(1998)124:9(846), 846–856.
- Loganathan, N., Poulos, H. G., and Xu, K. J. (2001). "Ground and pile-group responses due to tunnelling." *Soils Found.*, 41(1), 57–67.
- Losacco, N., Burghignoli, A., and Callisto, L. (2014). "Uncoupled evaluation of the structural damage induced by tunnelling." *Géotechnique*, 64(8), 646–656.
- Mair, R. (2013). "Tunnelling and deep excavations: Ground movements and their effects." *Proc., 15th European Conf. on Soil Mechanics and Geotechnical Engineering*, A. Anagnostopoulos, M. Pachakis, and C. Tsatsanifos, eds., IOS Press, Amsterdam, Netherlands, 39–70.
- Mair, R., and Williamson, M. (2014). "The influence of tunnelling and deep excavation on piled foundations." *Proc., 8th Int. Symp. on Geotechnical Aspects of Underground Construction in Soft Ground*, C. Yoo, S.-W. Park, B. Kim, and H. Ban, eds., Taylor & Francis, Seoul, 21–30.
- Mair, R. J. (1993). "Unwin memorial lecture 1992: Developments in geotechnical engineering research: Application to tunnels and deep excavations." *Proc. Inst. Civ. Eng. Geotech. Eng.*, 97(1), 27–41.
- Mair, R. J., Taylor, R. N., Burland, J. B., and Taylor, R. N. (1996). "Prediction of ground movements and assessment of risk of building damage due to bored tunnelling." *Proc., Int. Symp. on Geotechnical Aspects of Underground Construction in Soft Ground*, R. J. Mair and R. N. Taylor, eds., Balkema, Rotterdam, Netherlands, 713–718.

- Marshall, A., and Mair, R. (2011). "Tunneling beneath driven or jacked end-bearing piles in sand." *Can. Geotech. J.*, 48(12), 1757–1771.
- Marshall, A. M., Farrell, R., Klar, A., and Mair, R. (2012). "Tunnels in sands: The effect of size, depth and volume loss on greenfield displacements." *Géotechnique*, 62(5), 385–399.
- Marshall, A. M., and Haji, T. (2015). "An analytical study of tunnel-pile interaction." *Tunnelling Underground Space Technol.*, 45(Jan), 43–51.
- Marshall, A. M., Klar, A., and Mair, R. (2010). "Tunneling beneath buried pipes: View of soil strain and its effect on pipeline behavior." *J. Geotec. Geoenviron. Eng.*, 10.1061/(ASCE)GT.1943-5606.0000390, 1664–1672.
- Mroueh, H., and Shahrouh, I. (2002). "Three-dimensional finite element analysis of the interaction between tunneling and pile foundations." *Int. J. Numer. Anal. Methods Geomech.*, 26(3), 217–230.
- Namazi, E., and Mohamad, H. (2013). "Assessment of building damage induced by three-dimensional ground movements." *J. Geotech. Geoenviron. Eng.*, 10.1061/(ASCE)GT.1943-5606.0000822, 608–618.
- Ng, C., Soomro, M., and Hong, Y. (2014). "Three-dimensional centrifuge modelling of pile group responses to side-by-side twin tunnelling." *Tunnelling Underground Space Technol.*, 43(Jul), 350–361.
- Ng, C. W. W., Lu, H., and Peng, S. Y. (2013). "Three-dimensional centrifuge modelling of the effects of twin tunnelling on an existing pile." *Tunnelling Underground Space Technol.*, 35(Apr), 189–199.
- Potts, D. M., and Addenbrooke, T. I. (1997). "A structure's influence on tunnelling-induced ground movements." *Proc. Inst. Civ. Eng. Geotech. Eng.*, 125(2), 109–125.
- Son, M. (2015). "Response analysis of nearby structures to tunneling-induced ground movements in sandy soils." *Tunnelling Underground Space Technol.*, 48(Apr), 156–169.
- Soomro, M. A., Hong, Y., Ng, C. W. W., Lu, H., and Peng, S. (2015). "Load transfer mechanism in pile group due to single tunnel advancement in stiff clay." *Tunnelling Underground Space Technol.*, 45(Jan), 63–72.
- Takahashi, K., Fukazawa, N., Hagiwara, T., and Hosoda, M. (2004). "Observational control of slurry shield tunnels with super close spacing under the nearby bridge abutments loads." *Tunnelling Underground Space Technol.*, 19(4), 390.
- Taylor, R. N. (1995). "Tunnelling in soft ground in the UK." *Underground construction in soft ground*, A.A. Balkema, Rotterdam, Netherlands, 123–126.
- Vorster, T. E. B., Klar, A., Soga, K., and Mair, R. J. (2005). "Estimating the effects of tunneling on existing pipelines." *J. Geotech. Geoenviron. Eng.*, 10.1061/(ASCE)1090-0241(2005)131:11(1399), 1399–1410.
- White, D., Take, W., and Bolton, M. (2003). "Soil deformation measurement using particle image velocimetry (PIV) and photogrammetry." *Géotechnique*, 53(7), 619–631.
- Zhang, R. J., Zheng, J. J., Zhang, L. M., and Pu, H. F. (2011). "An analysis method for the influence of tunneling on adjacent loaded pile groups with rigid elevated caps." *Int. J. Numer. Anal. Methods Geomech.*, 35(18), 1949–1971.
- Zhou, B., Marshall, A. M., and Yu, H.-S. (2014). "Effect of relative density on settlements above tunnels in sands." *2014 GeoShanghai Int. Congress: Tunneling and Underground Construction*, Vol. 242, ASCE, Reston, VA, 96–105.